UNIVERSITY OF CALIFORNIA, SAN DIEGO

Dynamic Analysis of a 5 Megawatt Offshore Floating Wind Turbine

A Thesis submitted in partial satisfaction of the requirements

for the degree Master of Science

in

Structural Engineering

by

Evan Michael Harriger

Committee in charge:

Professor Qiang Zhu, Chair
Professor Ahmed-waeil M. Elgamal
Professor Francesco Lanza Di Scalea

2011

The Thesis of Evan Michael Harriger is approved, and it is acceptable in quality and form for publication on microfilm and electronically:

_____

_____

_____

Chair

University of California, San Diego

2011

TABLE OF CONTENTS

LIST OF FIGURES

LIST OF TABLES

ACKNOWLEDGEMENTS

I would like to thank Professor Qiang Zhu for allowing me to be involved in this research project and for his support as chair of my committee.

I would also like to thank Kourosh Shoele for all his contributions to this project. Without his answers to all my questions and expert advice, this research would have been much more difficult.

ABSTRACT OF THE THESIS

Dynamic Analysis of a 5 Megawatt Offshore Floating Wind Turbine

by

Evan Michael Harriger

Master of Science in Structural Engineering

University of California, San Diego, 2011

Professor Qiang Zhu, Chair

Offshore wind is a valuable source of renewable energy, as it is typically strong and steady. Turbines have been utilized offshore in parts of Europe and Asia, however only at shallow depths. Floating wind turbines must be implemented in deeper areas to be economical, but this technology is relatively new and untested.

This paper describes a numerical analysis model that can be used to investigate the motion of a 5 MW floating turbine subjected to ocean conditions. Prototype designs for a spar buoy and barge platform are studied. The stiffness and damping effects brought about by the mooring lines are evaluated using a dynamic cable model. A boundary element model is used to calculate added mass and damping effects, as well as the forces on the structure caused by the wave-body interaction. The governing equations of motion include all the added mass, damping and stiffness components in the frequency domain. Response of the structure is found by solving the governing equation combined with a wave spectrum to represent actual ocean wave fields. Approximate bending moments at the base of each design are found by inputting the predicted base motion into a linear modal analysis model created in SAP2000. Based on the results found in this paper, incoming waves cause much greater motion of the barge design, especially in the pitching direction.

Chapter 1

Introduction

1.1 Why offshore wind energy?

Offshore wind turbines have the potential to generate enormous amounts of energy. They are more effective than similar land-based turbines because offshore winds are more consistent and blow up to 25% stronger than onshore winds [1]. Efficiently harnessing this wind provides a renewable source of energy and helps to lessen the dependence on fossil fuels. This technology also has zero harmful emissions, which will aid in combating climate change [2]. In fact, each GW of clean wind power eliminates 1.8 million metric tons of harmful carbon emissions that would otherwise be generated from coal or natural gas production [3]. Another advantage of offshore wind energy is that production occurs in closer proximity to load centers, which allows for more efficient transmission.

1.2 History and background

While land-based wind turbines have been around for many years, offshore turbines are a relatively new concept. The first offshore projects began in Europe in 1990 [1]. The European Union has been in the forefront of developing this technology with completed projects in Belgium, Denmark, Finland, Germany, Ireland, the Netherlands, Norway, Sweden, and the United Kingdom. As of summer 2010, offshore turbines in Europe had a total generating capacity of 2,396 MW with many other projects in the planning stages [3]. Japan and China also started utilizing this technology in 2004 and 2007, respectively [2]. However, most of these early wind farms are similar in that they are located close to shore and in water depths of 30 meters or less [2].

The design of the support structure for each offshore turbine is dictated by the water depth. There are three different depth classes: shallow, transitional and deep. In the shallow water case, the turbine is rigidly fixed to the seafloor, using a monopole or foundation similar to those on land. At transitional depth, the structure is still rigidly connected to the sea bottom, but the support structure is usually wider in order to provide the needed stability and stiffness. Typical designs include a tripod or spaceframe [2]. Proven knowledge from both land based and shallow water installations has been adapted in the development of the support structure for the transitional case.

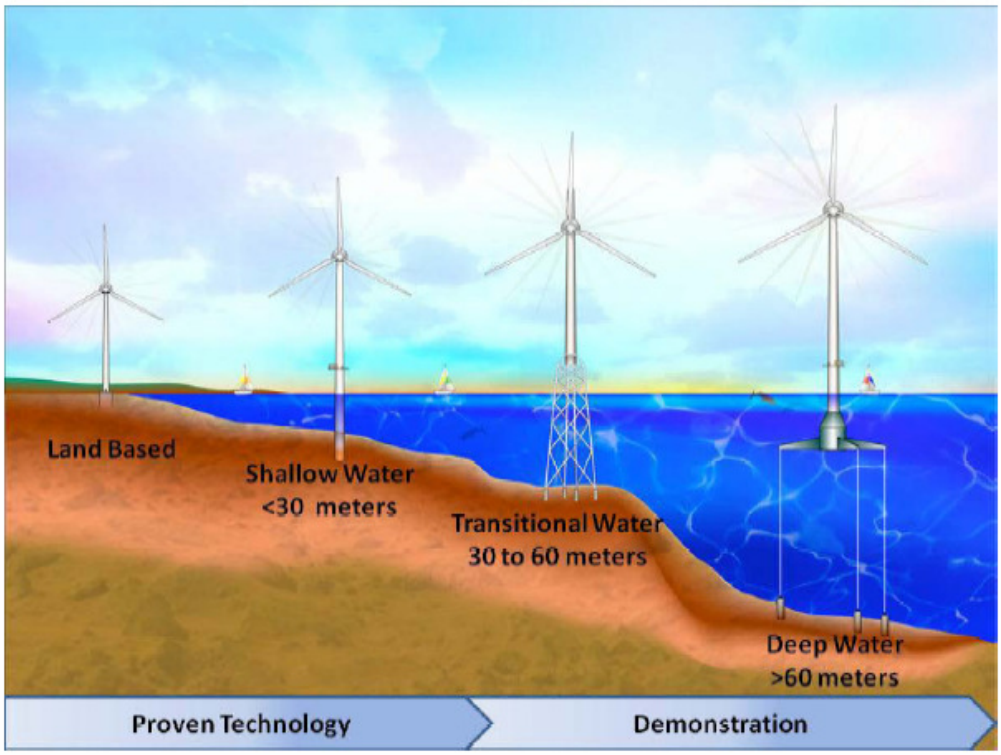

Figure 1.1: Offshore wind turbine classification [3].

The real technological challenges begin to surface when turbines are wanted in much deeper water. Using existing technology is not economically sensible in deeper locations because of the large cost of the support structure. Therefore, floating turbines are the alternative [1]. The turbines must also be much larger and capable of generating more power in order to offset the added expenses. Turbines as large as 10 MW have been proposed for offshore usage, which is much large than anything used on land [2].

There are different types of floating platform for these structures and three common configurations are shown in Figure 1.2. These concepts have been developed using knowledge gathered from the offshore industry. Each of these designs relies on a different primary source of stability. The ballast of the spar buoy, buoyancy forces

of the barge and mooring lines of the tension leg platform provide the majority of stabilization for each type of structure [4].

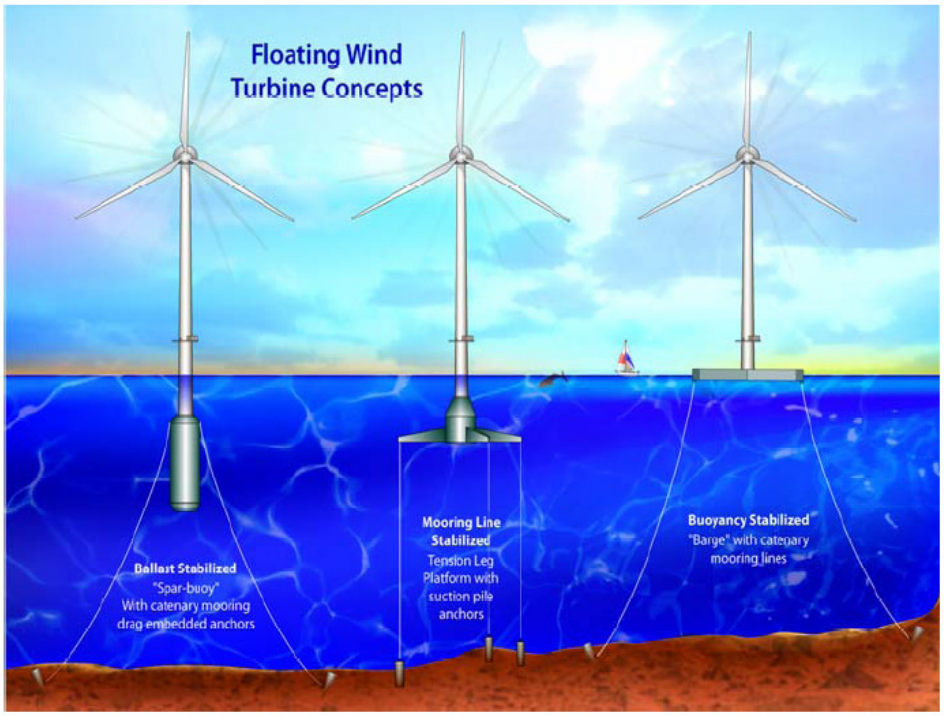

Figure 1.2: Alternative platform designs for floating turbines [4].

The Statoil Hywind project was launched in June 2009 off the coast of Norway at a depth of 220 m and is the first large scale floating wind turbine. This system is comprised of a 2.3 MW Siemens turbine supported by a 100 meter spar buoy. Three mooring lines are used to prevent drifting. The pilot project will be monitored over a two-year period to investigate the overall effects of wind and waves on the structure [5]. All results from this initial test will be important in the development and design of upcoming projects. The Hywind turbine will also uncover potential problems that exist with offshore wind energy. The information obtained will help to reduce the cost of all future floating wind turbines and allow this technology to be more attractive in the power market [6].

Figure 1.3: Hywind concept floating wind turbine [5].

1.3 Potential in United States

Although the United States does not currently have any offshore wind turbines in operation, this technology has the potential to revolutionize electricity production. It is estimated that the U.S. could generate 4,000 GW of energy by installing offshore turbines on the East and West Coast, Great Lakes, and Gulf of Mexico. This is more than four times the current generating capacity of the United States [2]. However, development of deep water technology is a hurdle that must be overcome as more than half of the potential energy would need to be generated in a water depth of over 60 meters. Figures 1.4 and 1.5 show the overlap of excellent wind resources and deep ocean depth, especially along the West Coast.

In the U.S. especially, it is extremely advantageous that offshore power production is in close proximity to the shore because coastal counties account for 53 % of the population of the United States [7]. In fact, the 28 contiguous states with coastline along the Pacific or Atlantic Ocean, Gulf of Mexico and Great Lakes are

majority consumers, using 78 % of the nation's electricity [3]. Energy produced offshore would therefore not need to be transmitted long distances in order to reach areas with the greatest electrical needs.

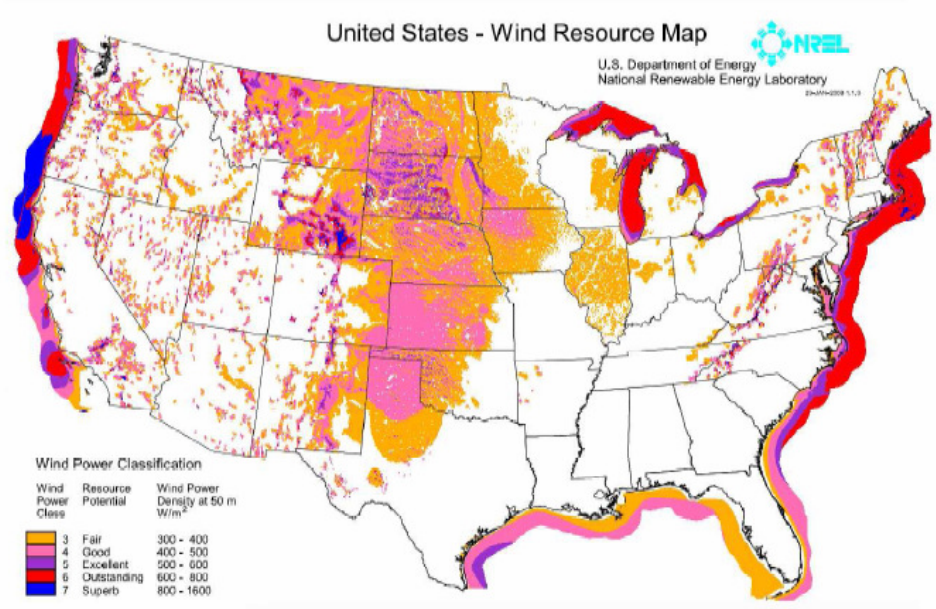

Figure 1.4: United States onshore and offshore wind resources [8].

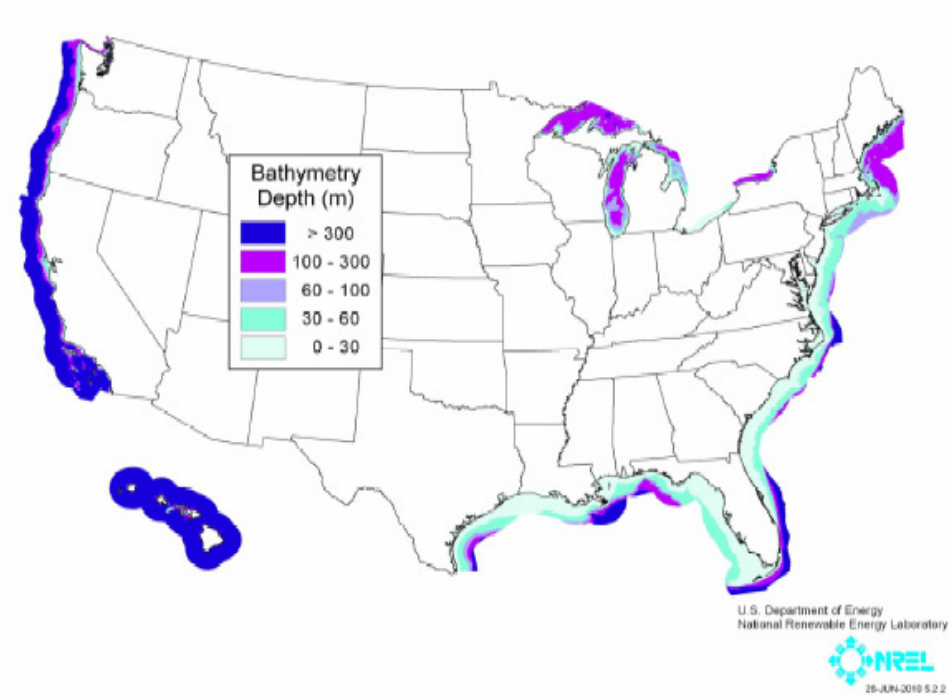

Figure 1.5: Water depths near U.S coastlines [8].

1.4 Objective

The objective of this paper is to describe a numerical analysis model that can be used to predict the motion and structural response of a 5 MW floating wind turbine. The study will be carried out for a spar buoy and barge design. These are two very different designs, the spar buoy having a small cross section and deep draft whereas the barge has a much larger cross section but shallow draft. These floating systems are subjected to more complicated loading conditions so examining the effects of waves and wind on each structure is essential for the development of this technology. Understanding the motion is critical as it can provide insight on issues like possible fatigue failures of the turbine [9]. This becomes more significant when there is additional motion of the support platform. There is also the potential for resonance in the turbine or mooring system brought about by oscillations caused by oncoming waves. Another important question to consider is how the motion of the turbine effects energy production [10]. These additional concerns must all be accounted for in the structure's design. Data from numerical analysis like this paper and actual experiments like the Hywind, can be combined with existing codes for land-based turbines and offshore structures to create industry standards. This would then provide engineers with the necessary background information needed in order to make this technology feasible and allow for widespread implementation of it.

Chapter 2

System properties

2.1 Spar buoy design

2.1.1 Floating platform

Table 2.1: Properties of support buoy.

Length	120 m
Top Diameter	6.5 m
Bottom Diameter	9.4 m
Mass	7,466,330 kg
Location of Center of Mass (below waterline)	89.92 m
Pitch Moment of Inertia (about CM)	4,229,230,000 kg·m²

The structure being analyzed is known as the OC3-Hywind concept and was designed by the National Renewable Energy Lab (NREL). The support platform utilizes the same spar buoy design as the Hywind pilot but has been modified to support a larger 5 MW turbine [12]. The overall length of the buoy is 120 m and it is designed so that the top 10 m will remain above the waterline. The diameter at the top

is 6.4 m and is constant over the first 14 m of the buoy. It is varies linearly over the next 8 m, increasing to 9.4 m. The diameter then is unchanged for the remaining length of the cylinder as shown in Figure 2.1.

The mass of the buoy is 7,466,330 kg, which includes enough ballast to generate the necessary buoyancy force to support the weight of the turbine. The center of mass is closer to the bottom of the structure at a depth of 89.92 m below the water surface. This helps with stability by always keeping the center of buoyancy above the center of mass. The moment of inertia about the center of mass in the pitching direction is 4,229,230,000 kg·m^2 [12].

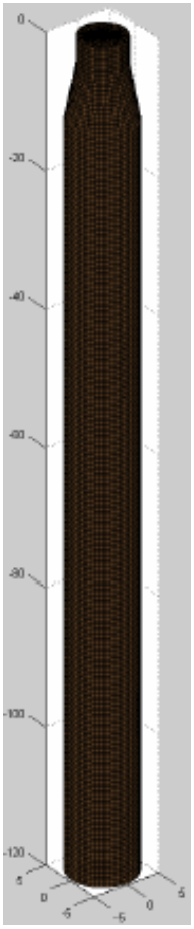

Figure 2.1: Spar buoy design [12].

2.1.2 Mooring lines

Table 2.2: Properties of buoy mooring lines.

Number of Lines	3
Depth of Connection at Buoy	70 m
Depth of Connection at Anchors	320 m
Angular Distribution of Lines	0°,120°,240°
Distribution Radius at Top	5.2 m
Distribution Radius at Bottom	853.9 m
Unstretched Length	902.2 m
Line Diameter	.09 m
Mass per Unit Length	77.7 kg/m
Bending Stiffness	20,000 $N \cdot m^2$
Stretching Stiffness	384,243,000 N

The mooring system consists of three cables that are equally spaced around the buoy. They are attached to the structure 70 m below the water surface and then anchored to the seafloor. In this specific design, the ocean depth has been assumed to be 320 m. The cables extend outward to a radius of 853.9 m at the connection to the seafloor. Orientation of these lines is shown in Figure 2.2.

The lines have an initial unstretched length of 902.2 m and a diameter of 0.09 m. The mass per unit length of these cables is 77.2 kg/m and weight in water per unit length is 698.1 N/m. The bending stiffness and stretching stiffness for each mooring line is 20,000 $N \cdot m^2$ and 384,243,000 N, respectively [12].

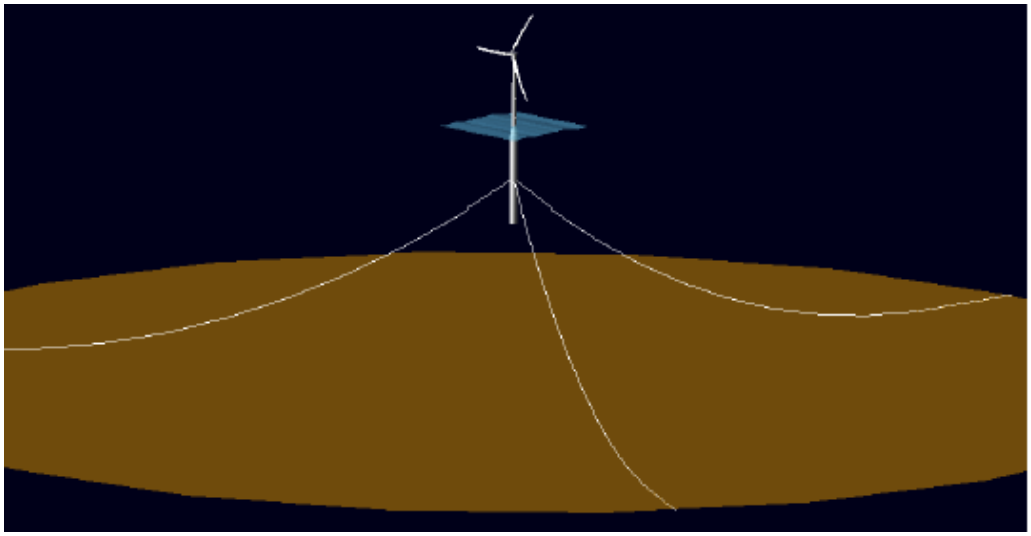

Figure 2.2: Mooring line configuration [12].

2.1.3 Wind turbine

Table 2.3: Properties of wind turbine.

Rating	5 MW
Control	Variable Pitch
Rotor Radius	63 m
Rated Wind Speed	11.4 m/s
Tower Height	77.6 m
Elevation of Tower Base (above waterline)	10 m
Tower Mass	249,718 kg
Rotor Mass	110,000 kg
Nacelle Mass	240,000 kg

The wind turbine attached to the support platform is the "NREL offshore 5-MW baseline wind turbine" [11]. It was developed for various studies conducted on offshore wind turbines. The 5 MW Reference design was created using two existing 5 MW prototypes, the Multibred M5000 and the REpower 5M. It is a three blade, horizontal axis turbine with variable blade pitch control. Each blade extends outward

a distance of 63 m and has a rated speed of 12.1 rpm. The system begins to generate power at a cut in wind speed of 3 m/s and stops at a cut out speed of 25 m/s.

The tower is attached to the buoy 10 m above the water surface which causes the top of the tower and rotor to be at a height of 87.6 m above the sea level. This dimensioning allows for sufficient clearance between the blade tips and extreme wave heights. The steel tower has a diameter of 6.5 m and wall thickness of 0.027 m at the base. Both of these dimensions taper to 3.87 m and 0.019 m at the top. The mass of the tower is 249,718 kg, which includes any additional weight from paint, bolts, welds and any other components. The rotor has a mass of 110,000 kg and the nacelle has a mass of 240,000 kg [11, 12]. When calculating the center of mass and moment of inertia for the entire system, the rotor and nacelle are simplified as point masses located at the top of the tower.

Figure 2.3: NREL 5 MW Reference Wind Turbine [12].

2.2 Barge design

2.2.1 Floating platform

Table 2.4: Properties of support barge.

Length	40 m
Width	40 m
Height	10 m
Mass	5,452,000 kg
Location of Center of Mass (below waterline)	0.2818 m
Pitch Moment of Inertia (about CM)	726,900,000 kg·m^2

This floating barge design was developed by ITI Energy. It is a square structure with side length of 40 m and a depth of 10 m. The platform is ballasted with seawater, resulting in a total weight of 5,452,000 kg and a draft of 4 m below sea level. The center of mass is 0.2818 m beneath the surface and the pitching moment of inertia about this point is 726,900,000 kg·m^2 [13].

2.2.2 Mooring lines

The barge concept utilizes 8 mooring lines to prevent drifting. Two lines are connected to the bottom of the barge at each corner. They radiate outward and are anchored at a position 45° apart. Assuming the ocean depth to be 150 m, each cable has an unstretched length of 473.312 m with about 250 m of the cable resting on the seafloor. To simplify analysis, the line resting on the seafloor was eliminated as it will have little effect considering only small displacements of the platform. Each cable has a diameter of 0.0809 m, mass per unit length of 77.2 kg/m and weight in water per unit length of 698.1 N/m. The bending stiffness of a single line is 20,000 N·m^2 and

stretching stiffness is 589,000,000 N [13]. Figure 2.4 shows the static positions of the mooring lines.

Table 2.5: Properties of barge mooring lines.

Number of Lines	8
Depth of Connection at Buoy	4 m
Depth of Connection at Anchors	150 m
Angular Distribution of Lines (top)	45°,45°,135°,135°, 225°,225°,315°,315°
Angular Distribution of Lines (bottom)	23.965°,66.035°,113.965°,156.035°, 203.965°,246.035°,293.965°,336.035°
Distribution Radius at Top	28.2843 m
Distribution Radius at Bottom	423.422 m
Unstretched Length	473.312 m
Line Diameter	0.0809 m
Mass per Unit Length	130.403 kg/m
Bending Stiffness	20,000 $N \cdot m^2$
Stretching Stiffness	589,000,000 N

2.2.3 Wind turbine

The same 5 MW reference wind turbine is used in this design, however there are slight modifications of the tower. The height of the tower was increased to 87.6 m in order to achieve the desired rotor height. The base of the tower has a slightly smaller diameter of 6 m but same wall thickness of 0.027 m. Both of these dimensions are linearly tapered to the same values at the top as in the previous case. The material properties remain unchanged and the resulting mass of this tower configuration is 347,460 kg. Rotor and nacelle masses are the same as given above.

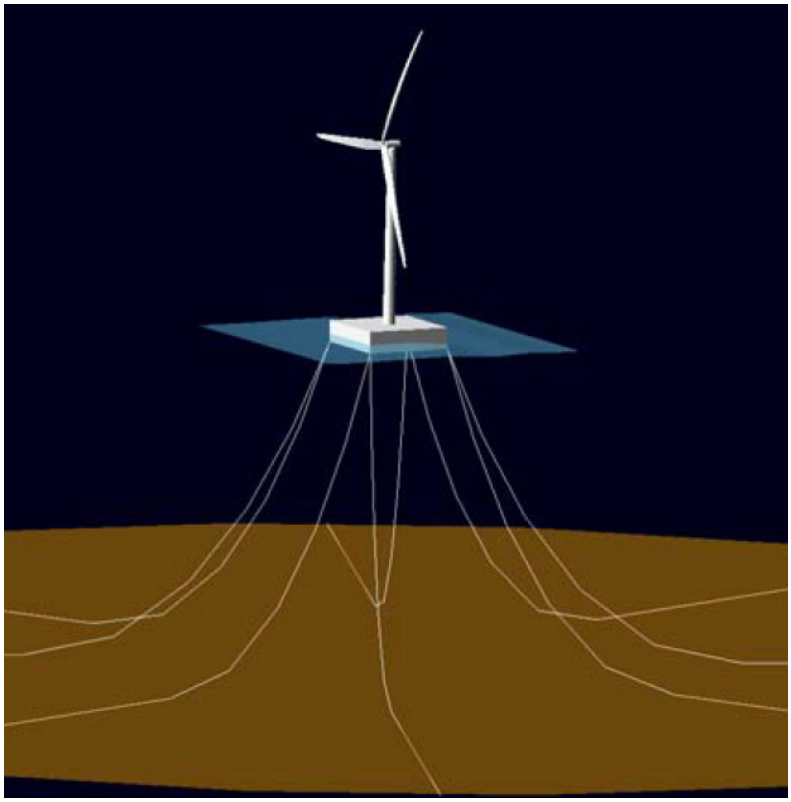

Figure 2.4: ITI Barge configuration [13].

Chapter 3

Mathematical model

3.1 Problem formulation

The mathematical model used in this paper was initially developed to study a 65 KW floating turbine system [10]. This approach to predict the response of the structure involves using a dynamic cable model to study the effects of the mooring lines, coupled with the wave-body interactions of the floating platform. The calculations for the cable and wave models are carried out in the frequency domain and only linear behavior is considered. This model does not take into account the aerodynamic forces of the rotating blades, as they occur at much higher frequencies than the wave forces on the platform.

The structure will be considered to have six degrees of freedom, three translational and three rotational that can be seen in Figure 3.1. In this analysis, the origin of the coordinate system is set to coincide with the center of the tower at the

water surface. Incoming waves are assumed to propagate in the x_1 direction. Only motion along the surging (x_1) and pitching (x_5) degrees of freedom will be considered, as these are most significant given the wave direction.

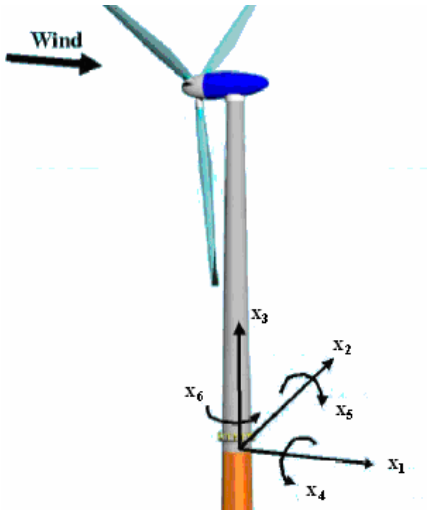

Figure 3.1: Floating turbine degrees of freedom [14].

The equations of motion for this system can be written as follows

$$\mathbf{M}\cdot\ddot{\mathbf{x}}+\mathbf{B}\cdot\dot{\mathbf{x}}+\mathbf{C}\cdot\mathbf{x}=\mathbf{F} \tag{1}$$

where $\mathbf{x}=\begin{Bmatrix}x_1\\x_5\end{Bmatrix}$, $\dot{\mathbf{x}}=\dfrac{\partial\mathbf{x}}{\partial t}$ and $\ddot{\mathbf{x}}=\dfrac{\partial^2\mathbf{x}}{\partial t^2}$. **M** is the mass matrix, **B** is the damping matrix and **C** is the stiffness matrix. The resulting force and moment caused by the waves on the structure is defined as $\mathbf{F}=\begin{Bmatrix}F_1\\F_5\end{Bmatrix}$. If motion is assumed to be harmonic in time with frequency ω, Equation 1 can be rewritten as

$$\left[-\omega^2\mathbf{M}+i\omega\mathbf{B}+\mathbf{C}\right]\cdot\mathbf{x}=\mathbf{F} \tag{2}$$

The mass, damping and stiffness matrices are comprised of the following components:

$$\mathbf{M} = \begin{bmatrix} M + \alpha_{11} & \alpha_{15} \\ \alpha_{51} & I_{55} + \alpha_{55} \end{bmatrix} \tag{3}$$

where M is the total mass of the system, I_{55} is the pitching moment of inertia with respect to the water surface. α_{ij} is the added mass coefficient calculated using the wave-body model with imposed motion in the i-th direction causing a response in the j-th direction. Because only two degrees of freedom are considered i=1,5 and j=1,5.

$$\mathbf{B} = \begin{bmatrix} B_{11} + \beta_{11} & B_{15} + \beta_{15} \\ B_{51} + \beta_{51} & B_{55} + \beta_{55} \end{bmatrix} \tag{4}$$

where B_{ij} and β_{ij} are the damping coefficients found using the cable and wave-body models respectively.

$$\mathbf{C} = \begin{bmatrix} C_{11} & C_{15} \\ C_{51} & C_{55} + K_{55} + Mgx_{cm} \end{bmatrix} \tag{5}$$

where C_{ij} is the cable stiffness, K_{55} is the hydrostatic stiffness, g is the acceleration due to gravity and x_{cm} is the location of the center of mass. Once the mass, damping and stiffness matrices are evaluated, the amplitude of motion can be found by solving Equation 2.

3.2 Cable model

The cable model as describe below was derived by Tjavaras *et al.* [15]. This approach is suitable for cables with nonlinear stress-strain relations and eliminates any error due to small tensions by considering bending stiffness. The following three assumptions were made during derivation:

• The cross-section is circular or annular and homogenous over the entire length

• The bending stiffness can be represented by the Euler-Bernoulli beam model

• Strain can be nonlinear as long as tension is a single value function of strain $T=f(\varepsilon)$

Each cable can be described in a fixed global or local Lagrangian coordinate system. The fixed system is represented by the unit vectors $\hat{i}$, $\hat{j}$ and $\hat{k}$. The local coordinate system varies along the cable and is composed of unit vectors in the tangential direction $\hat{t}$, normal direction $\hat{n}$ and bi-normal direction $\hat{b}$.

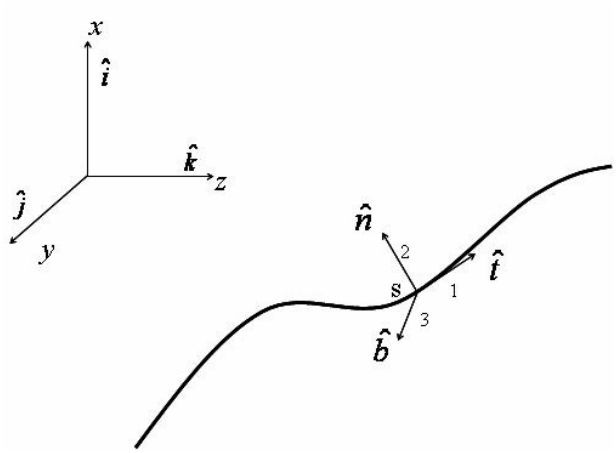

Figure 3.2: Global and local coordinate systems [16].

In order to transform between the two coordinates, there is a relation between the two systems given in the form of the rotation matrix **C**

$$\begin{bmatrix} \hat{t} \\ \hat{n} \\ \hat{b} \end{bmatrix} = \mathbf{C} \begin{bmatrix} \hat{i} \\ \hat{j} \\ \hat{k} \end{bmatrix} \tag{6}$$

The matrix **C** is evaluated using the Euler parameters formulation so all singularity is eliminated. This formulation states that any orientation of the local frame can be

achieved by a rotation of principle angle α about a principle vector $\hat{l}$. Knowing these two principle values, the four Euler parameters can be found

$$\beta = \begin{bmatrix} \beta_0 \\ \beta_1 \\ \beta_2 \\ \beta_3 \end{bmatrix} = \begin{bmatrix} \cos(\alpha/2) \\ l_x \sin(\alpha/2) \\ l_y \sin(\alpha/2) \\ l_z \sin(\alpha/2) \end{bmatrix} \tag{7}$$

The values calculated from Equation 7 are then used to evaluate the rotation matrix **C** using the following

$$\mathbf{C} = \begin{bmatrix} \beta_0^2 + \beta_1^2 - \beta_2^2 - \beta_3^2 & 2(\beta_1\beta_2 + \beta_0\beta_3) & 2(\beta_1\beta_3 - \beta_0\beta_2) \\ 2(\beta_1\beta_2 - \beta_0\beta_3) & \beta_0^2 - \beta_1^2 + \beta_2^2 - \beta_3^2 & 2(\beta_2\beta_3 + \beta_0\beta_1) \\ (\beta_1\beta_3 + \beta_0\beta_2) & 2(\beta_2\beta_3 - \beta_0\beta_1) & \beta_0^2 - \beta_1^2 - \beta_2^2 + \beta_3^2 \end{bmatrix} \tag{8}$$

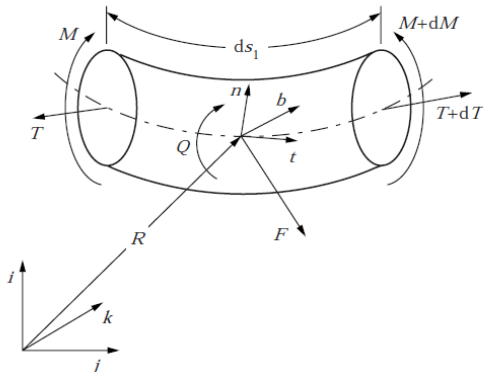

Figure 3.3: Infinitesimal cable segment [15].

The equations of motion can be derived by investigating an infinitesimal segment of cable of mass *m*. Newton's second law states that the sum of forces is equal to the mass times acceleration and the following equation is found by applying this law

$$m\left(\frac{\partial \mathbf{V}}{\partial t}+\omega\times\mathbf{V}\right)=\frac{\partial \mathbf{T}}{\partial t}+\Omega\times\mathbf{T}+(1+\varepsilon)\mathbf{F}_e \tag{9}$$

where $\mathbf{V}=u\hat{t}+v\hat{n}+w\hat{b}$ is the velocity, $\omega=\omega_1\hat{t}+\omega_2\hat{n}+\omega_3\hat{b}$ is the angular velocity and $\Omega=\Omega_1\hat{t}+\Omega_2\hat{n}+\Omega_3\hat{b}$ is the local curvature of the cable. ε is the strain and represented by the change in length over the initial length. The internal force in the cable is represented by the vector $\mathbf{T}=T\hat{t}+S_n\hat{n}+S_b\hat{b}$ where T is the tension and S_n and S_b are shear forces in the normal and bi-normal directions. $\mathbf{F_e}$ is the external forces which include all applied, gravity, hydrostatic and hydrodynamic forces. Morrison's equation is used to calculate the hydrodynamic force. Because the cables are submerged, the effective tension T_e must be used which accounts for the buoyancy force acting on the cable. Therefore, $T_e=T+(p_eA_1)/(1+\varepsilon)$ where p_e is the hydrostatic pressure and A_1 is the area of the cross section after stretching.

Another equation can be formulated by balancing the moments of the infinitesimal segment and results in the following

$$\frac{1}{(1+\varepsilon)^2}\frac{\partial \mathbf{M}}{\partial s}+\frac{1}{(1+\varepsilon)^2}\Omega\times\mathbf{M}+(1+\varepsilon)\hat{t}\times\mathbf{T}=0 \tag{10}$$

where vector **M** represents the internal moments of the segment. It is assumed that the moments are proportional to the curvature in each direction by the relation

$$\mathbf{M}=\begin{bmatrix}M_t\\M_n\\M_b\end{bmatrix}=\begin{bmatrix}GI_p\Omega_1\\EI\Omega_2\\EI\Omega_3\end{bmatrix} \tag{11}$$

where GI_p is the torsional stiffness and EI is the bending stiffness. This relationship is important to eliminate the number of unknowns, allowing for a unique solution to be found.

A third equation is found using the compatibility relation. The position vector $R(S,t)$ as shown in Figure 3.3 must be continuous with respect to both variables. The partial derivatives $\frac{\partial \mathrm{R}}{\partial s}$ and $\frac{\partial \mathrm{R}}{\partial t}$ must also be continuous. Therefore, the equations below can be formulated

$$\frac{\partial \varepsilon}{\partial t}\hat{t} + (1+\varepsilon)\omega \times \hat{t} = \frac{\partial \mathbf{V}}{\partial s} + \Omega \times \mathbf{V} \tag{12}$$

The initial assumption that tension T is a function of strain ε is used to eliminate the variable T and simplify the problem. Equations 9, 10 and 12 each have three components resulting in 9 equations but there are 13 unknowns. The relations between the space derivatives of the Euler parameters and the curvatures provide the final four equations needed to close the system of equations. Writing everything in vector form yields

$$\frac{\partial \mathbf{Y}}{\partial s} + \mathbf{M}(\mathbf{Y})\frac{\partial \mathbf{Y}}{\partial t} + \mathbf{P}(\mathbf{Y}) = 0 \tag{13}$$

where $\mathbf{Y} = [\varepsilon \quad \mathrm{S_n} \quad \mathrm{S_b} \quad \mathrm{u} \quad \mathrm{v} \quad \mathrm{w} \quad \beta_0 \quad \beta_1 \quad \beta_2 \quad \beta_3 \quad \Omega_1 \quad \Omega_2 \quad \Omega_3]^T$ and the components of **M** and **P** are defined using Equations 9, 10 and 12.

A numerical box method is used to solve Equation 13. The first step is to divide the cable into n_p -1 segments of length Δs using points k=1,2,3…,n_p. The length is variable for each segment and can be adjusted accordingly at critical points to produce more accurate results. Time is also divided into time steps where $t_i=t_{i-1}+\Delta t$.

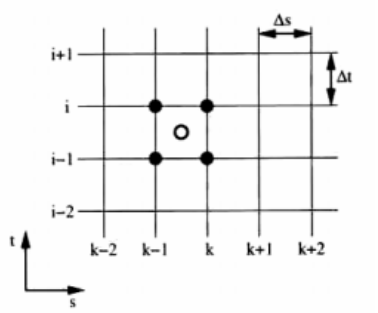

Figure 3.4: Example of "box" numerical method [16].

Using the box pictured above, the value of the center is defined as the average of the four corners. The partial derivatives with respect to s and t are defined to be the average slopes between the two points in that respective direction. Using these definitions, Equation 13 can be rewritten as

$$\begin{aligned} &2\Delta t\left(\mathbf{Y}_{k,i}-\mathbf{Y}_{k-1,i}-\mathbf{Y}_{k-1,i-1}\right) \\ &+\Delta s\left[\left(\mathbf{M}_{k-1,i}+\mathbf{M}_{k-1,i-1}\right)\left(\mathbf{Y}_{k-1,i}-\mathbf{Y}_{k-1,i-1}\right)+\left(\mathbf{M}_{k,i}+\mathbf{M}_{k,i-1}\right)\left(\mathbf{Y}_{k,i}-\mathbf{Y}_{k,i-1}\right)\right] \\ &+\Delta t\Delta s\left(\mathbf{P}_{k-1,i-1}+\mathbf{P}_{k-1,i}+\mathbf{P}_{k,i-1}+\mathbf{P}_{k,i}\right)=0 \end{aligned} \tag{14}$$

This equation can be solved for all points knowing the initial conditions, boundary conditions at each endpoint and the value of **Y** for each previous time step.

In order to calculate the stiffness and damping components of the mooring lines, the top of each cable was forced into motion. The specified motion represented the response of the cables due to harmonic oscillation of the floating platform in the surging and pitching degrees of freedom. A time-history response for the force in the x_1 direction and moment in the x_5 direction was found using the cable model. A Fourier transform was then performed to convert the results into the frequency domain. Assuming linearity, the damping component B_{ij} was calculated as the real part of the response divided by excitation amplitude and the stiffness component C_{ij} was the imaginary part divided by excitation amplitude.

3.2 Wave-body interaction model

A numerical boundary element method (BEM) was used to solve the wave-body interaction [10, 17, 18]. This method is based on potential theory, assuming the flow is inviscid, incompressible and irrotational. A Cartesian coordinate system is used with coordinates x, y and z corresponding to the x_1, x_2 and x_3 directions as shown in Figure 3.1. The free surface is represented by the z = 0 plane, with the fluid domain lying beneath at z < 0.

There exists a velocity potential $\mathbf{\Phi}(x,t)$ that can describe the motion of the fluid which satisfies the governing Laplace equation

$$\frac{\partial^2 \phi}{\partial x^2} + \frac{\partial^2 \phi}{\partial y^2} + \frac{\partial^2 \phi}{\partial z^2} = 0 \tag{15}$$

Assuming that the incoming waves are harmonic in time with frequency ω, the potential can be rewritten as

$$\Phi(x,t) = \mathrm{Re}\{\phi(x)e^{i\omega t}\} \tag{16}$$

which eliminates the time dependence of ϕ. The linear boundary condition at the free surface is

$$\frac{\partial^2 \phi}{\partial t^2} + g\frac{\partial \phi}{\partial z} = 0 \tag{17}$$

with g being the acceleration due to gravity. Because of the linearization of this problem, the velocity potential can be further broken down into the following

$$\phi(x) = A(\phi_I + \phi_S) + \phi_R \tag{18}$$

where ϕ_I is the incoming wave potential, ϕ_S is the diffraction potential and ϕ_R is the radiation potential. The first term in this decomposition presents the excitation caused by the waves and the second is the resulting added mass, damping and forces on the structure. ϕ_I is defined to be

$$\phi_I = (g/\omega)e^{kz+ikx} \tag{19}$$

where wavenumber *k* is defined as $k = \omega^2/g$ for deep water waves. Along the submerged surface of the body, the condition below must be satisfied relating the wave and diffraction potentials

$$\frac{\partial \phi_I}{\partial n} = -\frac{\partial \phi_S}{\partial n} \tag{20}$$

ϕ_R is defined as

$$\phi_R = \sum_{j=1}^{J} \eta_j \phi_j \tag{20}$$

where η_j is the complex amplitude of motion corresponding to the *j*-th mode. Typically, *j*=1, 2, 3, 4, 5, 6 for the six degrees of freedom but additional modes can be used to address structural deformations. For this problem however, only the response in the surging and pitching directions is used. The diffraction and radiation potentials must also satisfy a radiation boundary condition and the deep water condition given as

$$\frac{\partial \phi_{S,R}}{\partial z} \to 0 \text{ as } z \to -\infty \tag{21}$$

By discretizing the floating structure into flat panel sections, the theory mentioned above can be used to solve for the added mass and damping coefficients

and also the forces caused by wave excitations. In order to check the wave-body model, the case of a floating hemisphere was investigated. Results from the model were compared to asymptotic predictions calculated by Hulme [18]. There was little discrepancy in the results, furthermore validating the accuracy of the model [10].

Ocean waves are not made up of just a single frequency wave, but instead are the superposition of multiple waves with varying frequencies and wavelengths. In order to account for this characteristic, a wave spectrum must be used [20].

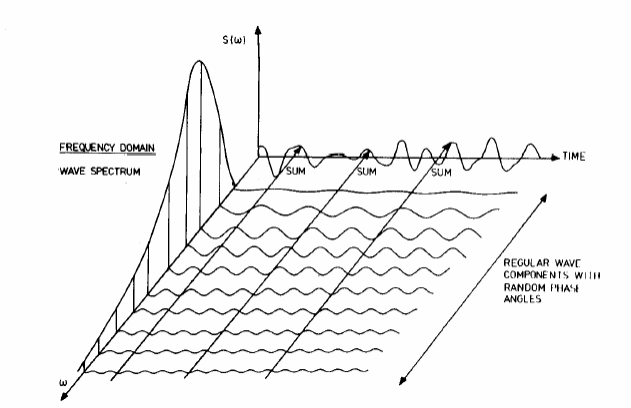

Figure 3.5: Wave spectrum for ocean waves [17].

The Bretschneider spectrum is used for deep water waves, propagating in one direction with unlimited fetch. An energy density function $S(\omega)$ is given as

$$S(\omega) = \frac{1.25}{4}\frac{\omega_m^{\,4}}{\omega^5} H_S^{\,2} \exp\left[-1.25\left(\frac{\omega_m}{\omega}\right)^4\right] \tag{22}$$

where ω_m is the modal frequency and H_S is the significant wave height [21]. Using the Pierson-Moskowitz relationship for fully developed seas, the modal frequency is defined as

$$\omega_m = 0.4\sqrt{\frac{g}{H_S}} \tag{23}$$

The actual wave field is determined using the summation of multiple waves at different frequencies. Assuming that the frequency range is divided into a sequence of N elements such that $\omega_i = \omega_{i-1} + \Delta\omega$, an amplitude factor A_i for each frequency is calculated using the energy density function and the equation below

$$\frac{1}{2} A_i^{\,2} = S(\omega_i)\Delta\omega \tag{24}$$

Finally, the free surface elevation ξ is found by summing all of the frequencies

$$\xi = \sum_{i=1}^{N} A_i \sin(\omega_i t - k_i x + \phi_i) \tag{25}$$

where k_i is the wavenumber found using the dispersion relation for frequency ω_i. ϕ_i is the phase of the wave and is chosen at random for this approximation.

Chapter 4

Results

4.1 Spar buoy design

The total mass of the system is M=8,066,048 kg and the moment of inertia calculated about the free surface in the pitching degree of freedom is I_{55}= 6.456×10^{10} kg·m^2. The cable model was evaluated for a frequency range of 0.01 Hz to 3 Hz, which encompasses the frequencies of a normal wave field in the ocean. Because of symmetry of the mooring system, the cross damping and stiffness terms are equivalent (B_{15}=B_{51} and C_{15}=C_{51}). The components obtained from the cable model are shown in Figure 4.1. It is clear that the mooring lines have three natural frequencies in this range as shown by the spikes in the damping and stiffness. At 0.24 Hz, 1.25 Hz and 2.48 Hz, resonance occurs causing an increased response. The lowest natural frequency is of the most concern as oscillations of the cables from incoming waves at this frequency would lead to amplified forces on the structure. However, higher

frequency vibrations, such as those caused by the rotating blades, could also cause resonance of the cables and highlight the importance of considering the dynamic behavior of the mooring lines.

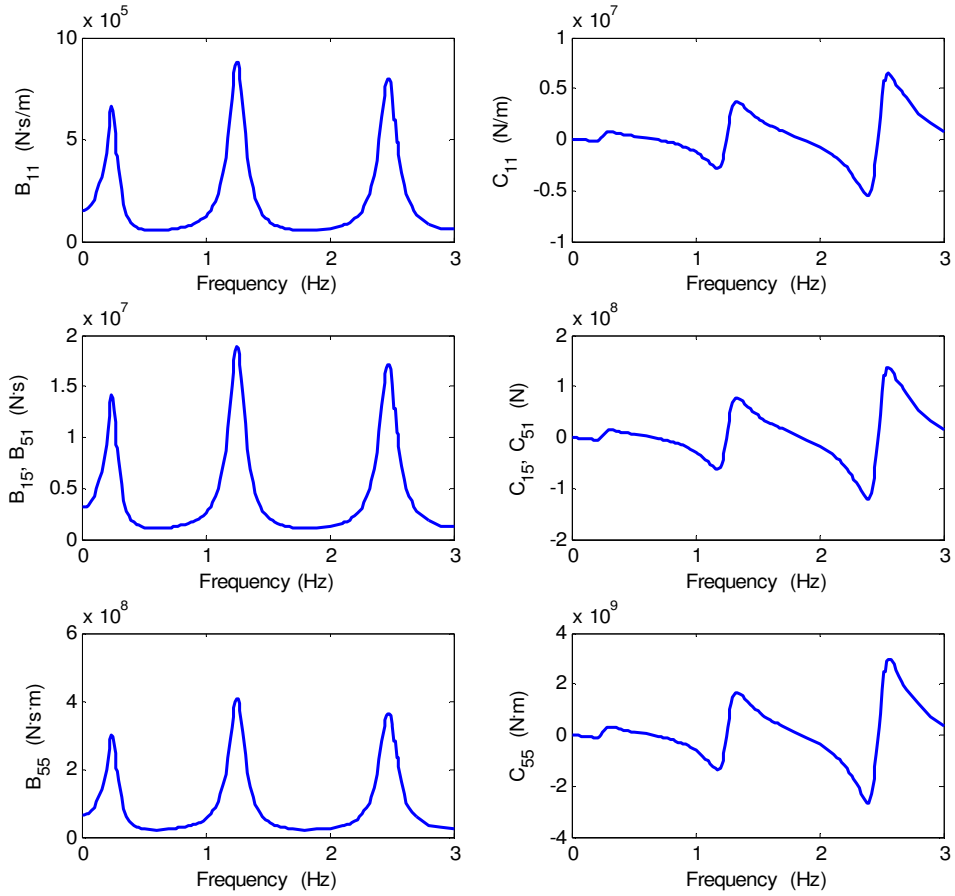

Figure 4.1: Damping (B_{ij}) and stiffness (C_{ij}) cable coefficients for the spar buoy design.

The wave-body interaction model was also run for incoming waves within the same frequency range. The added mass and damping components are pictured in Figure 4.2. Once again the cross terms are equivalent due to symmetry of the system, $\alpha_{15}=\alpha_{51}$ and $\beta_{15}=\beta_{51}$. These values are governed by the geometry of the structure. The

spar buoy has a hydrostatic pitching stiffness found to be $K_{55} = -5.001\times10^{9}$ N·m. The forces on the structure as a result of unit amplitude wave excitation in the surging and pitching directions are pictured in Figure 4.3. Because these values are complex, they have both real and imaginary components. All of the results from the wave model closely coincide with values published in an earlier NREL study [12].

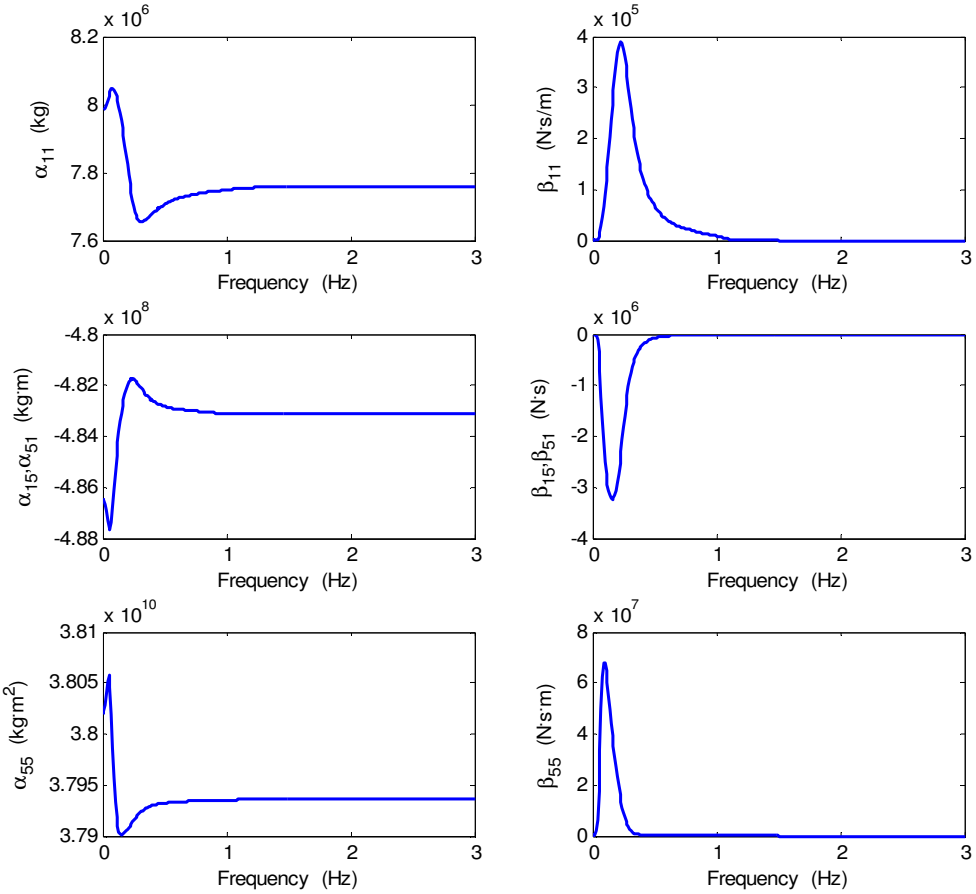

Figure 4.2: Added mass (α_{ij}) and damping (β_{ij}) coefficients caused by incoming waves on the spar buoy design.

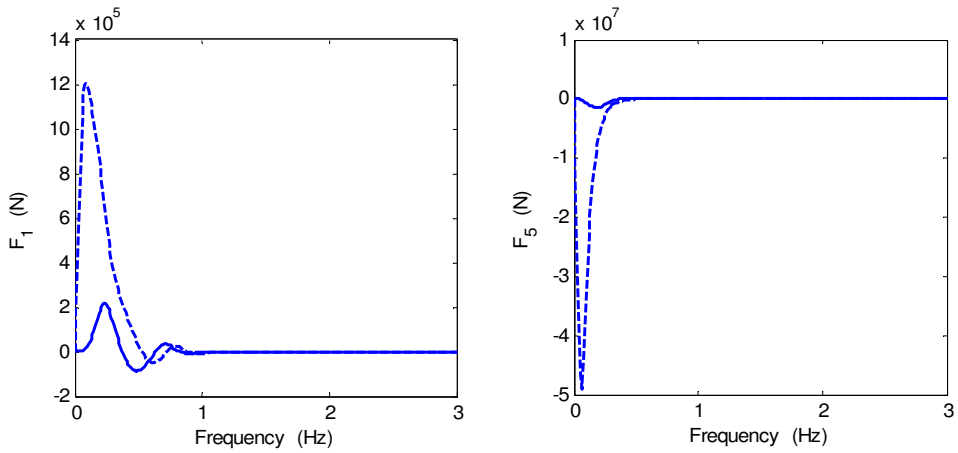

Figure 4.3: Real (solid) and imaginary (dashed) parts of wave excitation forces on spar buoy.

In this analysis, the significant wave height was assumed to be 7.5 m. This wave height represents rather extreme ocean conditions characterized as a sea state of 7 [22]. The Bretschneider wave spectrum, as defined by Equation 22, is shown below.

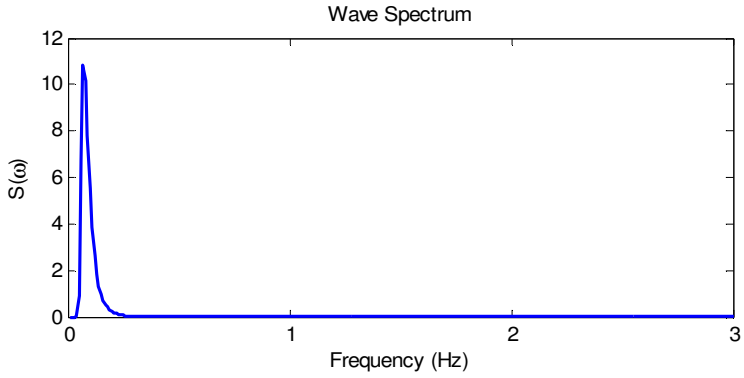

Figure 4.4: Wave spectrum for significant height 7.5 m.

The amplification factors for each specific frequency were calculated from the spectrum. Combining these values with the governing equation of motion allow for the amplitude of surging and pitching response at the water surface to be calculated. This dynamic response is plotted in Figure 4.5. Maximum amplitude for pitching

motion is much less than surging. Resonance of the mooring system is illustrated by the second smaller peak in the pitching response.

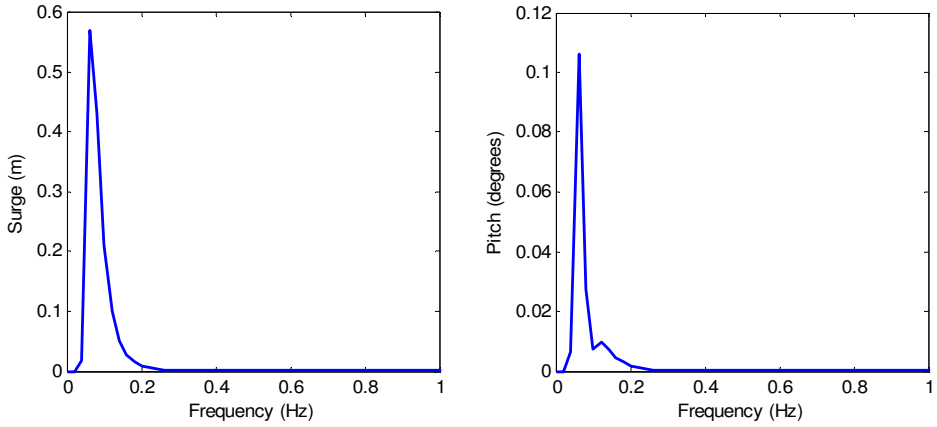

Figure 4.5: Amplitude of response of the spar buoy system.

A time history approximation for the motion at the base of the turbine was also calculated using Equation 25. It is important to note that the wave spectrum does not address the phase of the waves, so the phase has been assigned at random in making the transformation from frequency to time domain. This randomness included in the approximation does little to change the magnitude of motion though. Based on the results in Figures 4.5 and 4.6, it is clear that the spar buoy design is not susceptible to large pitching motions. Instead, most of the wave energy results in horizontal translation of the system. This is mainly due to the high moment of inertia of the design and small surface boundary on the water plane. These factors help to resist rotation and limit the influence of the waves on the support platform.

A model of the tower was created in SAP2000 in order to calculate the structural response of the turbine. The base was assumed to be fixed and the rotor and nacelle were idealized as point masses applied at the top of the tower. SAP2000 has

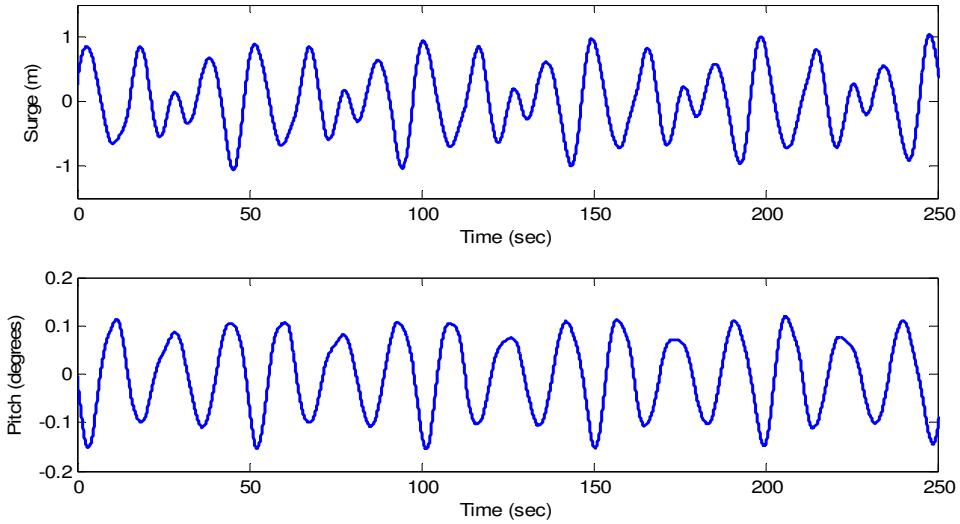

Figure 4.6:. Time history of base motion for spar buoy configuration.

the capability of performing a linear time-history modal analysis. This feature is often used to study the effects of earthquakes on a structure by using actual ground motion data. For this analysis, the same approach was used except the predicted base motion of the turbine was imported into the model. The bending moments at the base are shown in Figure 4.7. These results illustrate that the incoming waves generate cyclic forces on the turbine with the maximum moment at the base around 2,500 kN·m.

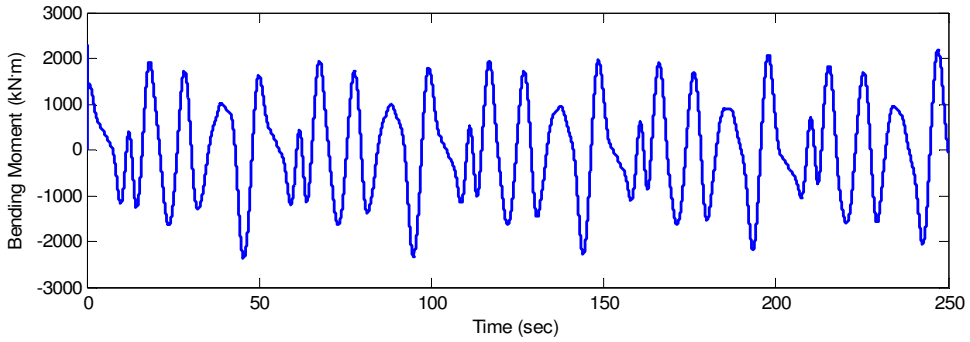

Figure 4.7: Resultant moment at base of tower caused by motion of spar buoy.

4.2 Barge design

The total mass of the barge configuration is M= 6,149,460 kg and the pitching moment of inertia calculated about the free surface is I_{55}= 4.637×10^{9} kg·m^2. The cable model was evaluated for the same frequency range as previously used. This system also is symmetric about the defined coordinate system so B_{15}=B_{51} and C_{15}=C_{51}. Once again, resonant responses were seen when the cables were excited near their natural frequency of 2.08 Hz as seen in Figure 4.8.

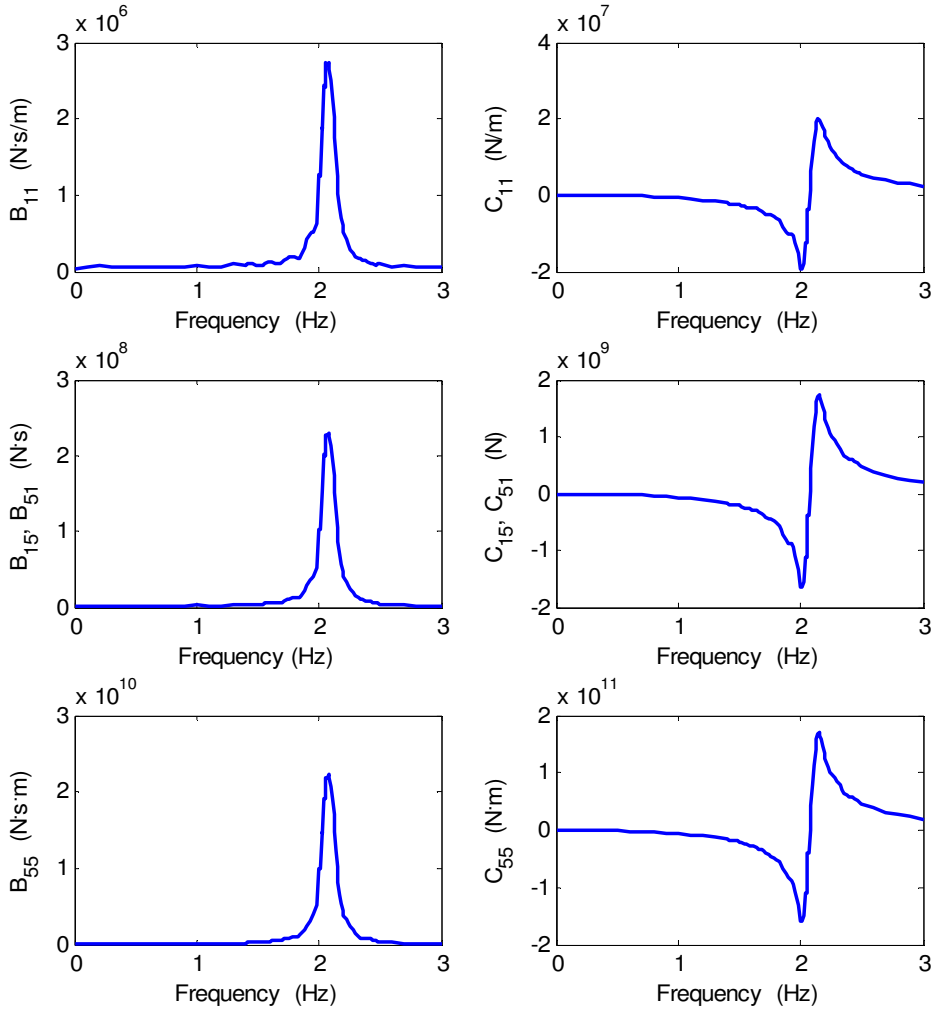

Figure 4.8: Damping (B_{ij}) and stiffness (C_{ij}) cable coefficients for barge design.

This further strengthens the argument that static approximations do not accurately represent the behavior of these mooring lines.

Figure 4.9 depicts the calculated added mass and damping components with equivalent cross terms $\alpha_{15}=\alpha_{51}$ and $\beta_{15}=\beta_{51}$. The larger cross section of this design causes more variation in these terms. $K_{55}= 2.024\times10^{9}$ N·m for the barge. Resulting forces on the barge due to wave excitations of unit amplitude are plotted in Figure 4.10.

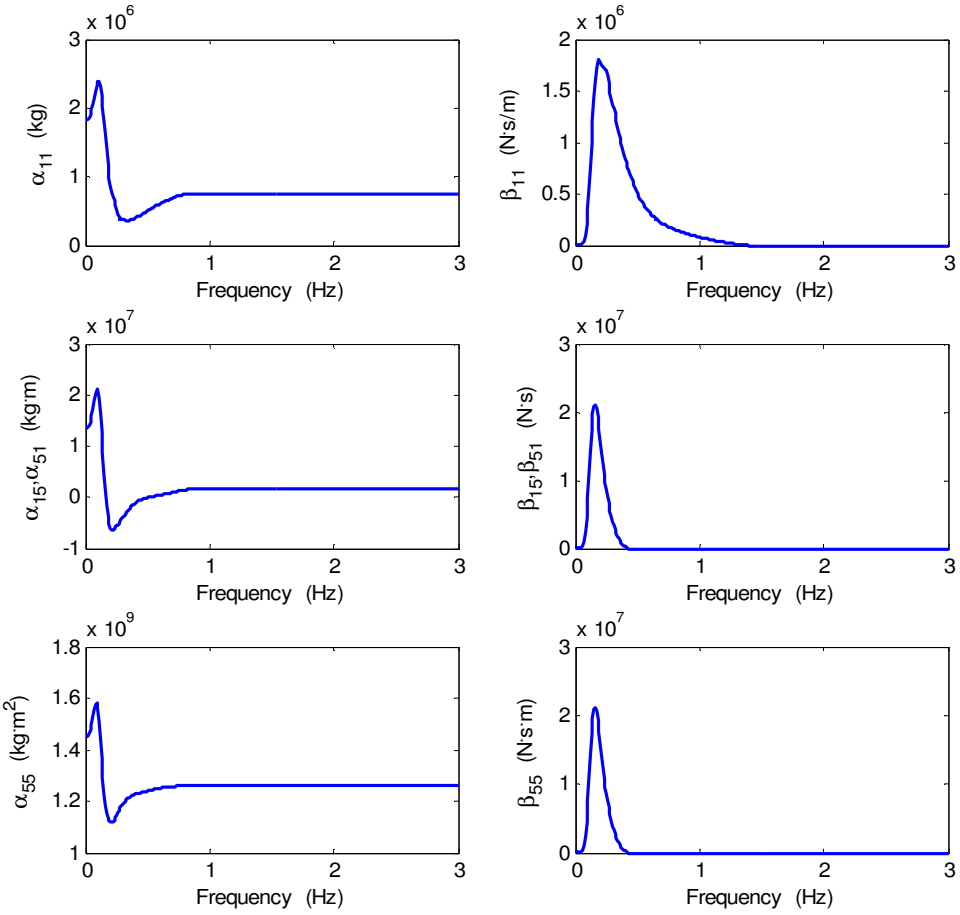

Figure 4.9: Added mass (α_{ij}) and damping (β_{ij}) coefficients caused by incoming waves on the barge design.

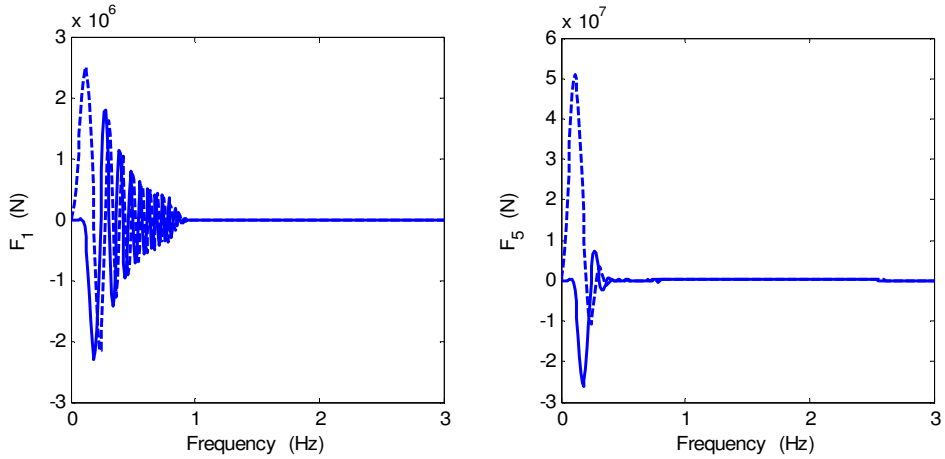

Figure 4.10: Real (solid) and imaginary (dashed) parts of wave excitation forces on barge.

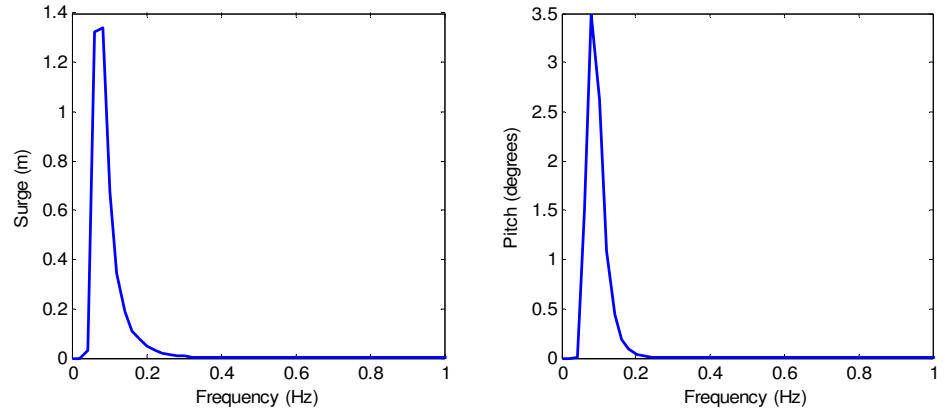

Figure 4.11: Amplitude of response of the barge system.

A significant wave height of 7.5 m was again used so the wave spectrum remains unchanged. The predicted response was found as illustrated above in Figure 4.11. The time history approximation of motion is plotted in Figure 4.12. These results show that waves of this height cause much greater motion of the barge, especially in the pitching degree of freedom. The pitching is in the magnitude of a few degrees, whereas it was only a fraction of a degree for the spar buoy. The barge

has a much larger area along the water surface which results in the waves having a much greater influence on the structure. This platform also lacks the deep draft to resist pitching.

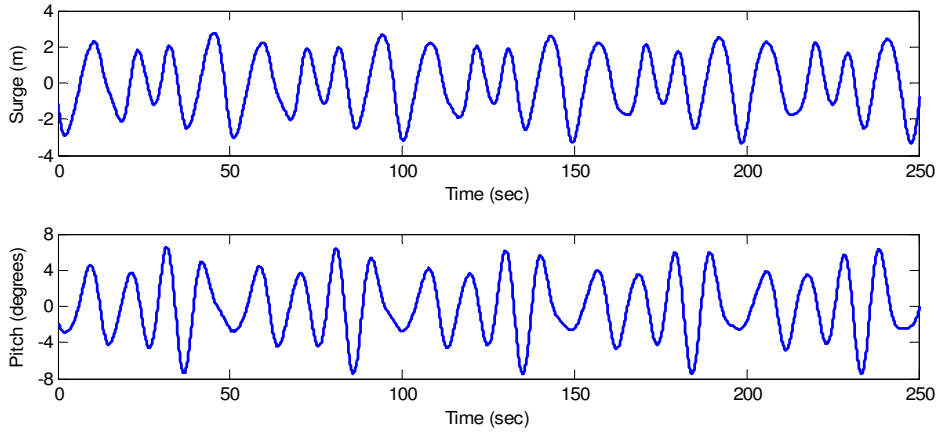

Figure 4.12: Time history of base motion for barge configuration.

A linear modal analysis in SAP2000 calculated the predicted bending moment at the tower base as seen in Figure 4.13. The amplified base motion generates more significant forces in the structures. In this case, moments at the base of the tower reach an excess of 50,000 kN·m.

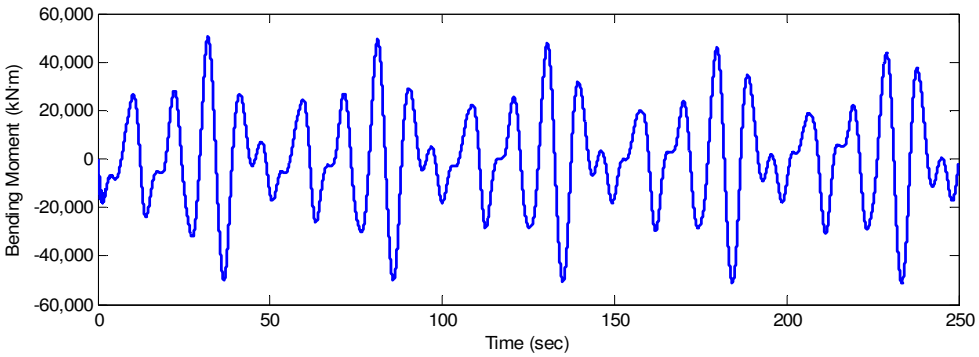

Figure 4.13: Resultant moment at base of tower due to motion of barge.

Chapter 5

Conclusion

5.1 Conclusions and discussions

The numerical model described in this paper predicts that a 5 MW floating wind turbine supported by the ITI Barge design is susceptible to greater surging and pitching motions than the same turbine attached to the OC3-Hywind spar buoy when exposed to extreme wave conditions. Furthermore, additional motion caused by incoming waves results in larger forces on the structure as proven by the amplified moments at the base of the barge turbine. The fatigue life of wind turbines is a major design consideration due to cyclic loading induced by the rotating rotors [23]. Therefore, any added forces from the motion of the support platform will have a detrimental effect, reducing the fatigue life of the structure. All of the excess motion can also be problematic for the control system and all other moving parts of a turbine.

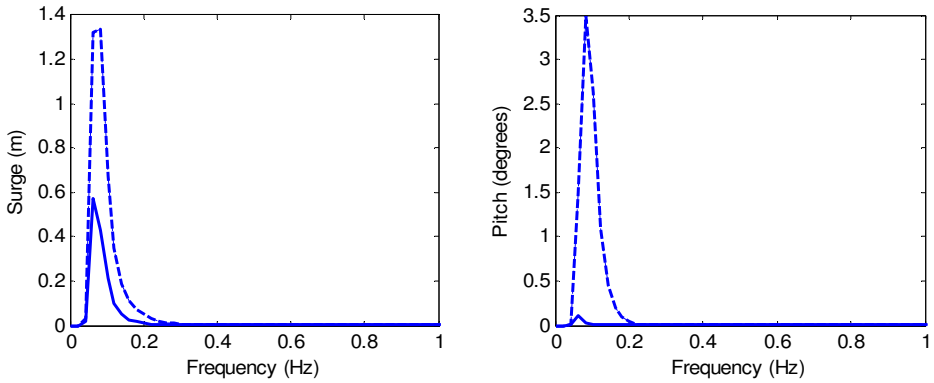

Figure 5.1: Comparison of response for spar buoy (solid) and barge (dashed).

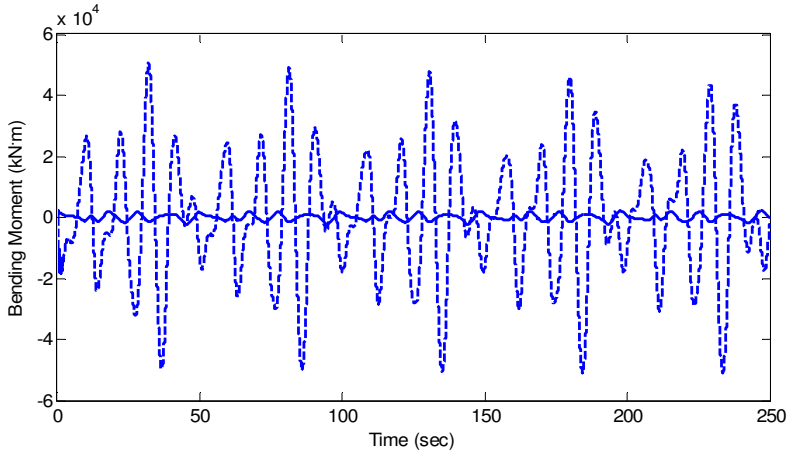

Figure 5.2: Comparison of base bending moment for spar buoy (solid) and barge (dashed).

While the response to wave excitation of a floating wind turbine is an important factor in the design of these structures, reducing the cost of such systems is essential for the utilization of this technology. The barge design has the lowest construction and installation costs. These structures can be built on land, utilizing assembly line production, and then floated out to their final location. This drastically simplifies the installation process and saves time and money. On the other hand, the exaggerated motion of these systems requires a more robust design to compensate for the higher forces and increases the cost of the turbine [4]. A way to address this issue

is to use a more advanced barge design. One such example is the "Pneumatically Stabilized Platform" which uses a series of open cylinders and the mobility of buoyancy air to lessen the influence of waves on the platform [24]. However, this concept has yet to be proven on a large scale and would also add to the cost and complexity of construction.

Assembly of the spar buoy design is much more complicated. If construction is completed on land, the unballasted structure must be towed out lying horizontal and then righted at the desired location. The other option is to assemble the system at sea. Both of these methods require advanced equipment at the installation site which generates large costs [25]. A very calm sea state is also required so delays are inevitable while waiting for ideal ocean conditions [4]. The constructability and installation of these structures is a very big issue and should be considered together with the structural performance and cost in order to determine the most sensible design.

5.2 Suggested future work

The analysis method described in this paper provides introductory insight about the behavior of offshore floating wind turbines. It can be expanded to incorporate additional degrees of freedom and provide results for other wave directions. This is most important for the barge because the hydrodynamic properties of this platform depend on wave orientation. Additional designs, such as the Dutch tri-

floater and tension leg platform, should also be evaluated and their performance analyzed.

A more advanced analysis tool would also include the aerodynamics of the turbine and address all nonlinear behavior. Such a model needs to be evaluated in the time domain because the frequencies of the wind and wave effects are much different. The cable model described in Section 3.1 can be useful because it is solved in the time domain and capable of analyzing nonlinear deformation. A more advanced wave-body interaction model is needed to take into account both linear and nonlinear effects as a function of time, not frequency. Aerodynamics of the turbine can be evaluated using methods such as the FAST Code [26]. All of these models must then be coupled together in order to accurately represent the entire system.

References

1. Clarke, Steven, Fara Courtney, Katherine Dykes, Laurie Jodziewicz, and Greg Watson. *U.S. Offshore Wind Energy: A Path Forward*. Working paper. U.S. Offshore Wind Collaborative, October 2009.

2. Musial, Walter, and Bonnie Ran. *Large-Scale Offshore Wind Power in the United States: Assessment of Opportunites and Barriers*. Tech. no. NREL/TP-500-40745. Golden, CO: National Renewable Energy Laboratory, September 2010.

3. Rock, Mary, and Laura Parsons. *Offshore Wind Energy*. Washingto, DC: Environmental and Energy Study Institute, October 2010.

4. Butterfield, Sandy, Walt Musial, and Jason M. Jonkman. *Engineering Challenges for Floating Offshore Wind Turbines*. Tech. no. NREL/CP-500-38776. Golden, CO: National Renewable Energy Laboratory, September 2007.

5. "Hywind – the World's First Full-scale Floating Wind Turbine." Statoil, 14 Oct. 2009. Web. 30 Mar. 2011. <http://www.statoil.com/en/TechnologyInnovation/NewEnergy/RenewablePowerProduction/Offshore/Hywind/Pages/HywindPuttingWindPowerToTheTest.aspx>.

6. Savenije, Laurens B. *Modeling the Dynamics of a Spar-type Floating Offshore Wind Turbine*. Thesis. TU Delft and Siemens Wind Power, 2009.

7. Crossett, Kristen M., Thomas J. Culliton, Peter C. Wiley, and Timothy R. Goodspeed. *Population Trends Along the Coastal United States: 1980-2008*. Rep. National Oceanic and Atmospheric Administration, September 2004.

8. Schwartz, Marc, Donna Heimiller, Steve Haymes, and Walt Musial. *Assessment of Offshore Wind Energy Resources for the United States*. Tech. no. NREL/TP-500-45889. Golden, CO: National Renewable Energy Laboratory, June 2010.

9. Withee, Jon E. *Influence of Wave Modeling on the Prediction of Fatigue for Offshore Wind Turbines*. Thesis. Massachusetts Institute of Technology, 2004. Cambridge, MA.

10. Shoele, Kourosh, Ian Prowell, Ahmed Elgamal, and Qiang Zhu. "Dynamic and Structural Modeling of a Floating Wind Turbine." *International Journal of Offshore and Polar Engineering*(2011).

11. Jonkman, Jason M., Sandy Butterfield, Walter Musial, and G. Scott. *Definition of a 5-MW Reference Wind Turbine for Offshore System Development*. Tech. no. NREL/TP-500-38060. Golden, CO: National Renewable Energy Laboratory, February 2009.

12. Jonkman, Jason M. *Definition of the Floating System for Phase IV of OC3*. Tech. no. NREL/TP-500-47535. Golden, CO: National Renewable Energy Laboratory, May 2010.

13. Jonkman, Jason M. *Dynamics Modeling and Loads Analysis of an Offshore Floating Wind Turbine*. Tech. no. NREL/TP-500-41958. Golden, CO: National Renewable Energy Laboratory, October 2007.

14. Withee, Jon E. *Fully Coupled Dynamic Analysis of a Floating Wind Turbine System*. Ph.D. Dissertation. Massachusetts Institute of Technology, 2004. Cambridge, MA.

15. Tjavaras, AA, Zhu, Q, Liu, Y, "Triantafyllou, MS, and Yue, DKP (1998). The mechanics of highly-extensible cables." *J Sound Vib*, Vol 213, No 4, pp 709-737.

16. Zhu, Qiang. "Chapter 4." SE 215 Cable Structures. University of California, San Diego. Lecture.

17. Faltinsen, O. M. *Sea Loads on Ships and Offshore Structures*. Cambridge: Cambridge UP, 1990.

18. Lee, C.-H., and J. N. Newman. "Computation of Wave Effects Using the Panel Method." Ed. S. Chakrabarti. *Numerical Models in Fluid-Structure Interaction* (2004).

19. Hulme, A. "The Wave Forces Acting on a Floating Hemisphere Undergoing Forced Periodic Oscillations." *Journal of Fluid Mechanics* 121.-1 (1982): 443.

20. Stewart, Robert H. *Introduction to Physical Oceanography*. College Station, TX: Texas A & M University, 2005.

21. Ochi, Michel K. *Ocean Waves The Stochastic Approach*. Cambridge: Cambridge UP, 1998.

22. Lee, W. T., W. L. Bales, and S. E. Sowby. *Standardized Wind and Wave Environments for North Pacific Ocean Areas*. Rep. no. A393951. Washington, DC: David W Taylor Naval Ship Research and Development Center, 1985.

23. Hau, E. *Wind Turbines: Fundamentals, Technologies, Application, Economics*. Berlin: Springer, 2006.

24. "PSP Technology." *Float Incorporated*. Web. 7 May 2011. <http://floatinc.org/PSPTechnology.aspx>.

25. Henderson, Andrew R., David Witcher, and Colin A. Morgan. "Floating Support Structures Enabling New Markets for Offshore Wind Energy." Proc. of European Wind Energy Conference 2009, Marseille, France. Gerrad Hassan.

26. Jonkman, Jason M., and Marshall L. Buhl Jr. *FAST User's Guide*. Tech. no. NREL/EL-500-38230. 6th ed. Golden, CO: National Renewable Energy Laboratory, August 2005.